IJAME

Int. J. of Applied Mechanics and Engineering, 2026, vol.31, No.1, pp.75-91
DOI: 10.59441/ijame/214980

STUDY OF THE FRACTURE FACIES WHEN DRILLING C-ORTHOCRYL CARBON-RESIN COMPOSITE MATERIAL FOR ORTHOPEDIC PROSTHESIS

F. Mesrafet[1*], Y. Menail[1], K. Chaoui[1] and D. Bouhafara[2]
[1]Mechanics of Materials & Plant Maintenance Research Laboratory (LR3MI), Mechanical Eng. Dept., Badji Mokhtar University, Sidi Amar Campus, P.O. Box 12, 23005, Annaba, Algeria
[2]National Higher School of Technology and Engineering, Laboratory of Energy Systems Technologies (LTSE), 23005, Annaba, Algeria
E-mail: farouk.mesrafet@univ-annaba.dz

Polymeric composites are increasingly used in orthopedic devices due to their high strength-to-weight ratio. However, machining, particularly drilling, remains a challenge because of high material costs and insufficient studies of drilling-induced damage in carbon-orthocryl composites. This study examines the mechanical behavior and micro-damages associated with drilling in prosthetic socket materials. Specimens *3 mm* thick were produced by infusion moulding and tested using static tensile and Charpy impact tests, followed by scanning electron microscopy (SEM) for damage characterization. Drilled specimens revealed a *29.64%* higher elastic modulus compared to conventional ones, while their ultimate tensile strength was *17.42%* lower. The average impact toughness was measured at *0.075 J/mm²*. SEM analysis revealed various degradation modes, including resin breakage, fiber rupture, intralaminar, translaminar, and interlaminar delamination, with poor resin-fiber wetting identified as a key defect. These results fill a gap in understanding the machinability of carbon-orthocryl composites and provide practical insights into improving molding techniques, notably increasing the amount of retarder, providing a pathway for enhancing carbon c-orthocryl socket machinability for drilling.

Key words: drilling, mechanical testing, SEM, delamination, injection molding, orthopedics.

1. Introduction

20 to *50* million non-fatal injuries occur each year worldwide following road accidents [1-3] and more than *1.2* million deaths, according to the World Health Organization [4]. Following these accidents, people with mobility impairments require orthopedic prostheses that have evolved from unsuitable wood to heavy metal to composite prostheses, which are now light, comfortable, and even intelligent. The design of orthopedic prostheses in composite materials [5, 6], requires an in-depth study, concerning the shape, the resistance [7, 8], the convenience and the lifespan over the past decades, Fewer studies have been conducted to assess the mechanical properties and microscopic damage of the socket of an orthopedic prosthesis produced through infusion molding, despite their significance for patients' daily activities. One of the primary reasons for this gap is the high cost of materials, fiber limitations such as low impact strength, low damage tolerance, etc., and the shortage of trained professionals [9, 10]. The prostheses require a primary machining step following infusion molding. Drilling was selected because it is one of the most common and clinically relevant machining processes in orthopedic applications, particularly during the assembly and prosthesis fixation (hip and knee riveting parts). The process is directly related to withstanding body weight, where controlled drilling is required to ensure precise dimensions and maintain the mechanical integrity of the prosthesis's structure [11]. During these processes, they undergo different constraints [12-14] which risk affecting their integrity and their lifespan. A mechanical study of the materials proves to be necessary [15-17]. To characterize the composite material, determine its resistance [18-21], and identify its defects, destructive tests and microscopic research

* To whom correspondence should be addressed

(SEM) were conducted, aiming to increase the lifespan of the prostheses [22, 23]. This study is part of a business-university relationship between the University of Annaba (LR3MI Laboratory) and the company ONAAPH (National Office of Apparatus and Accessories for Disabled People). It was the subject of one of the primary challenges in the fabrication of prosthetic sockets within the medical sector. This study aims to identify and characterize the damages surfaces specifically matrix cracking, delamination, decohesions, and ruptures of both the matrix and fibers [24-27], induced in carbon fiber and c-orthocryl resin composites before and after the drilling process of prostheses furthermore the relation between delamination and static testing is evident as established in previous research with the tensile strength deceases with the increase of the delamination in the drilled hole where the failure occurs in the specimen [28-32], on the other hand, the selection of appropriate resin-to-hardener ratios and the curing conditions in acrylic resin composites significantly impacts the microscopic structure and delamination behavior during the manufacturing of carbon fiber composites a recent studies indicates that a stoichiometric balance leads to optimal crosslinking density, enhancing mechanical properties and reducing porosity, which are crucial for preventing premature delamination. An optimal resin-to-hardener ratio results in superior interfacial bonding. This, in turn, enhances load transfer between the fibers and the matrix. The smoother delamination surfaces that occur under stress are a clear indicator of this improved bond integrity [33-34]. Increasing the hardener content can enhance the curing kinetics, resulting in a more homogenous and dense cross-linked structure, and the transition from Mode I to Mode II delamination involves varying stress responses, heavily influenced by the mechanical properties conferred by the acrylic resin's composition [35-36]. Although carbon c-orthocryl is a key material in the production of high-cost orthopedic prostheses, it remains subject to damage despite compliance with manufacturing protocols [37]. No prior investigations have specifically examined the microscopic fracture mechanisms that cause this degradation under typical molding conditions of this composite. This research aims to investigate the underlying fracture mechanism before and after drilling the prostheses, enhancing the molding techniques by increasing the amount of retarder, and improving the long-term durability by minimizing delamination and strengthening the orthopedic prostheses.

2. Materials and methods

In this study several steps were deployed to fabricate the laminate composite according to manufacture specifications [37] the carbon composite was composed of a weight fraction of *35%* carbon woven tissue and *63%* of c-orthocryl resin 617H55, adding *2%* hardener powder 617P37 at a ratio of approximately *100:2* by

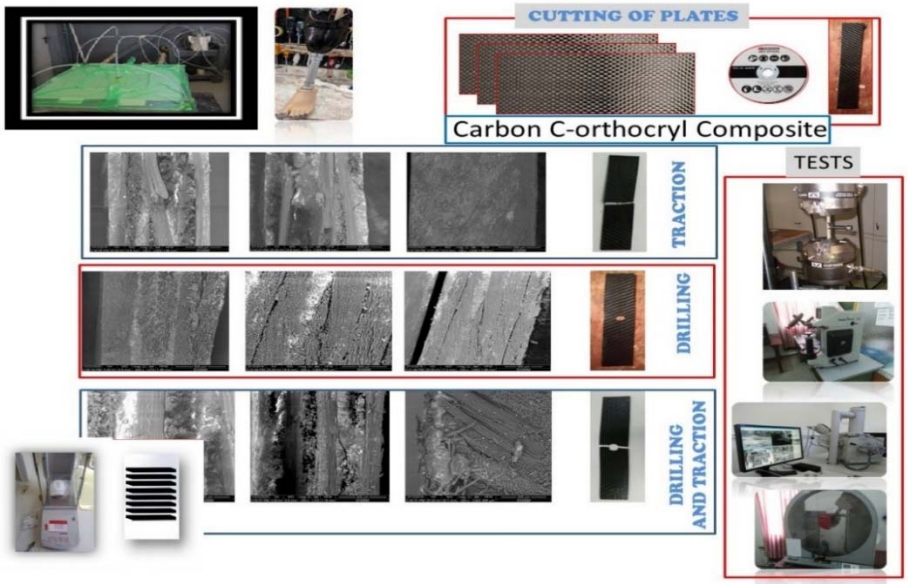

Fig.1. Manufacturing process for the carbon c-orthocryl composite.

weight (*2%* hardener)[38]. Laminated composite plates were stacked together by the vacuum infusion process with three layers of carbon, with a vacuum of *0.8* bar and a polymerization in an oven at *80°C* for *8* hours in an autoclave to facilitate the curing of the composite layers also reducing the generated porosity between the stacks, Fig.1 shows an explanation of the manufacturing process. These guidelines provide a consistent baseline for laboratory (onnaph) processing of carbon-orthocryl composites, ensuring both safety during curing and reproducibility of the mechanical performance [39].

2.1. Test plates

After polymerization, the plates were sectioned into test specimens of $220\times30\times2\ mm^3$ as per Standard ISO527-4 [40] for tensile testing; on the other hand, for impact testing (Charpy), $70\times10\times3$ according to Standard ISO 179-1 [41]. All material characteristics are summarized in Tab.1.

Tab.1. A summary of the material characteristics for the fabricated composite specimens.

Fiber	Weaving	Surface density $\left[g/m^2\right]$	Mass fraction [%]	Mixing ratio by weight	Curing conditions	Supplier
Carbon	woven 616G12	*245*	*35*	*100:2*	$T = 80°C$ $t = 8\,hrs$	Otto Bock (Duderstadt, Germany)
Resin	Acrylic c-orthocryl 617H55	-	*63*			
Hardener	617P37	-	*2*			
Sample	Layer	weight $[g]$	dimension $\left[mm^3\right]$			
	3	*12*	$220\times30\times2$			

2.2. Machine

The tensile tests were conducted on a Zwick/Roell universal machine model Z050, equipped with a *50 kN* force cell (Kennesaw, USA), as shown in Fig.2. The tests were performed at a loading speed of *2 mm/min* under laboratory conditions at room temperature. The test concluded following a substantial decrease in the applied load. Engineering stress-strain data can be derived from the load-displacement information recorded by the testing machine; the number of tests is limited due to the high cost of the material. The tensile modulus is determined by calculating the slope of the resulting stress-strain curve, the stress-strain curve calculated, and tensile strength and modules following the following Eq.(2.1) of CFRP for both of the specimens drilled and conventional, according to [40], can be calculated within a strain range from *0.0005* to *0.0025*. The details of the specimens before and after the test are shown in Fig.2(b-c), B. Huang investigated the tensile properties of the unidirectional CFRP plates with different lengths. Among these specimens, for the *150 mm* length, the tensile strength σ_{max} results vary from *2819 MPa* to *2598 MPa* [42], also demonstrated that intralaminar and interlaminar defects arise during static tensile testing of carbon fiber reinforced polymers (CFRP) as a result of macroscopic voids present between the layers. These voids create regions of stress concentration, which can significantly compromise the material's tensile resistance. Therefore, it is imperative to minimize the occurrence of such voids during the Manufacturing process of the composite [43]. All the results are summarized in Tab.2. The tensile stress-strain curve is illustrated in Fig.6.

$$E = \frac{\Delta\sigma}{\Delta\varepsilon}. \tag{2.1}$$

2.3. Protocol

The protocol to be followed was to divide the specimens into four lots. The first lot serves as a control Fig.2(a), the second will be subjected to a static tensile test Fig.2(b), the third will be drilled and subjected to a static tensile test Fig.2(c) and the fourth will be drilled by *8 mm* HSS twist drill bit Fig.2(d), the four specimens will be examined under the SEM electron microscope to detect the various defects existing after molding and the damages generated within the material by the drilling and tensile tests and to find the necessary solutions [18-22]. SEM images were taken using a high-resolution microscope vacuum system QUANTA 250 from FEI Company (Hillsboro, Oregon, USA). SEM observation of the damaged areas around the drilled holes revealed an obvious delamination concentration around this area. Furthermore, another shear crack appeared, indicating fiber failure in the direction of the applied tensile force.

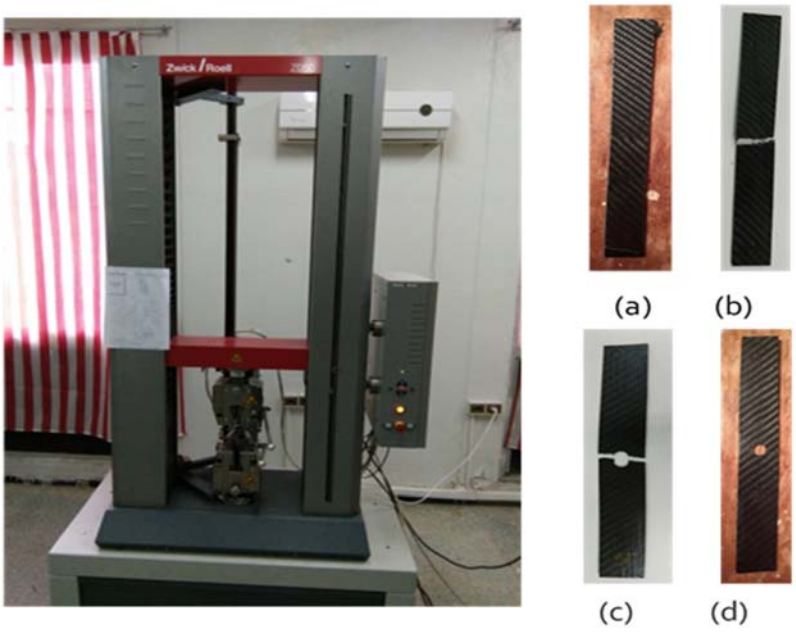

Fig.2. Different specimens and tensile machine Zwick/Roell Z050.

2.4. Charpy test resilience

The primary challenge in testing composites using the Charpy impact test is the complexity of failure modes, which often include delamination, matrix fracture, and fiber tearing. Additionally, delamination tends to decrease as the thickness of the laminate increases the goal from the test is to determine CFRP resistance to impact and the absorbed energy calculated with formula (2.2) following the previous studies [44, 45] the specimens were made According to [41] with dimension $77\times10\times3\ mm$, the specimens were cut using a diamond saw, impact device is Zwick/Roell HIT50P testing machine with an impactor energy level of *50* joule and a constant mass of *60 kg* and pendulum length *800 mm* and constant speed with a fixture stand and support base the specimen were placed in the front of the impactor to insure complete contact between impactor and specimen Fig.3, all the results are summarized in Tab.3.

$$E = \frac{W}{S_0}. \tag{2.2}$$

The specimen was classified and arranged along with the test arrangement, then carefully removed from the fixture after the test was completed. The specimen breaking is shown in Fig.6.

Fig.3. Zwick/Roell impact testing machine.

3. Results and discussion

3.1. Control specimens

We cut the control specimen in the longitudinal, transverse, and frontal directions, as shown in Fig.4. This cutting allows us to know the internal structure of the material and to detect possible molding defects along the various facies and fiber orientation across the plies. It exposes the fibers with a significant amount of c-orthocryl resin.

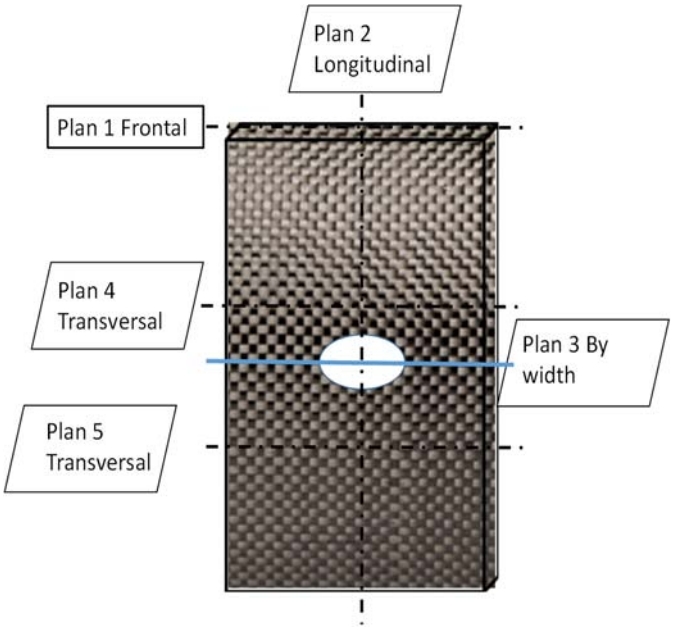

Fig.4. Different surfaces according to the cross-sectional planes of the tensile specimen.

3.1.1 The tensile test properties:

The tensile test results for the carbon fiber c-orthocryl resin composite show that the regular sample has an average tensile strength σ_{max} of *437.539 MPa*, an average Young's modulus *E* of *35.811 GPa*, as shown in Tab.2 based on the linear part of the stress-strain curve illustrated in Fig.5. The strain to failure is *1.7%*, which is typical of brittle behavior. Many factors can have significant impacts on the tensile strength of CFRP, including the environmental conditions and how it is processed mechanically. Li *et al*. [46] examined the impact of environmental conditioning on CFRP, demonstrating that tensile strength decreases with extended exposure to hydrothermal conditions, suggesting more significant effects on tensile strength when sustained loads are combined with hydrothermal aging. Additionally, the drilling process can cause damage mechanisms like delamination and micro-cracking, which change the material's tensile characteristics. Ueda *et al*. observed that drilled specimens frequently exhibit reduced tensile strengths relative to their non-drilled equivalents, ascribing this phenomenon to the onset of damage mechanisms during the drilling process [47]. Drilling an *8 mm* hole in the specimens creates a stress concentration that reduces the average σ_{max} by *17.42%* (to *361.286 MPa*) and the strain to failure by more than *52%* (to *0.8%*). The discontinuity serves as a crucial initiating point for crack propagation and early fracture, emphasizing the composite's vulnerability to geometric defects and the necessity of incorporating such characteristics in structural design. Evidence indicates that the drilling procedure influences both the load-bearing capacities and the strain properties of the CFRP matrices [48].

Tab.2. Mechanical properties of conventional and drilled carbon c-orthocryl specimens.

Conventional specimens	Tensile strength σ_{max} (MPa)	Young modulus E (GPa)
1	*474.085*	*34.340*
2	*470.887*	*40.089*
3	*416.992*	*36.037*
4	*388.195*	*32.779*
Average	*437.539*	*35.811*
Drilled specimens		
1	*379.798*	*55.111*
2	*342.775*	*46.896*
Average	*361.286*	*51.003*

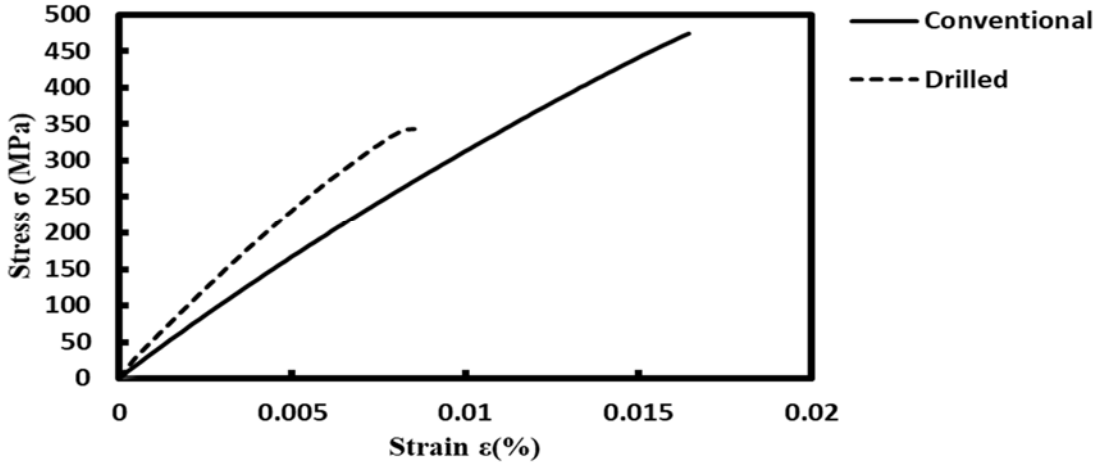

Fig.5. Tensile stress-strain curve for the carbon c-orthocryl composite.

3.1.2. The impact test properties

The Charpy impact test results show that the carbon c-orthocryl specimens absorbed between *1.899 J* and *2.668 J* of energy before fracture, dissipated through mechanisms such as fiber breakage, matrix cracking, and delamination. Normalizing by the initial cross-sectional area yields impact toughness values ranging from *0.068* to *0.086* J / mm^2 , as shown in Tab.3 with an average of *0.075* J / mm^2 across the five specimens. The consistency of these values supports the reliability of the dataset and indicates that the material possesses moderate resistance to fracture under high-strain-rate loading. The specimens after breaking are shown in Fig.6. These findings underscore both the potential of CFRP for lightweight structural applications and its inherent susceptibility to impact damage, emphasizing the importance of toughness characterization in prosthesis design. Curing conditions, including time, temperature, and the specific environment, have a significant effect on the mechanical properties of CFRP. Mahfoud and Harb explored how varying curing cycles can influence the performance of carbon fiber composites, noting that optimizing the cure cycle can lead to enhanced mechanical properties. However, their study primarily focused on wave modes during curing rather than directly demonstrating enhanced impact resistance [49]. Similarly, the resin-hardener ratio plays an important role in determining the physical characteristics of the hardened composite. Zhang *et al*. reported that the addition of carbon nanotubes (CNTs) can catalyze the curing process, resulting in improved mechanical properties, including impact strength [50]. They highlighted that the optimal ratio of resin to hardener affects the degree of cross-linking, which is crucial for the final product's load-bearing capability. Moreover, the curing degree directly correlates with the mechanical performance of CFRP composites. Ye *et al*. observed that higher degrees of curing lead to notable improvements in flexural strength and impact resistance of epoxy-based CFRP composites, with increases in impact strength up to *82.9%* when novel curing agents were introduced [51].

Tab.3. Impact test results for CRFP specimens.

Specimens	Speed $v\ (m/s)$	Surface $S_0\left(mm^2\right)$	$W\ (J)$	$W / S_0\left(J / mm^2\right)$ AVR
1	*3.807*	*30.914*	*2.668*	*0.086*
2	*3.807*	*27.678*	*1.899*	*0.068*
3	*3.807*	*31.950*	*2.196*	*0.068*
4	*3.807*	*25.310*	*1.899*	*0.075*
5	*3.807*	*29.431*	*2.251*	*0.076*

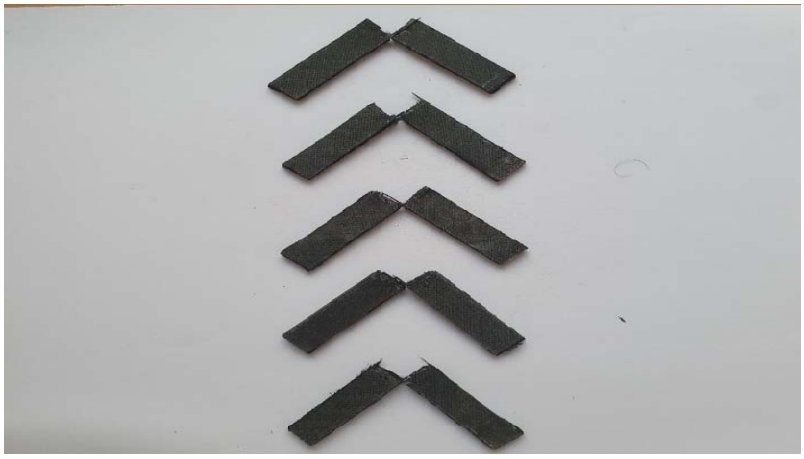

Fig.6. Charpy specimen after breaking.

3.2. Standard specimens before static tensile testing

The three SEM images in Fig.7 effectively provide an overview of the composite material, carbon fiber, and c-orthocryl resin. Figure 7A, (F1), (F2) shows a significant defect inside the specimen in the frontal plane. Some of the fiber bundles are not immersed in the resin. This lack of resin will weaken the material and reduce its cohesion. Previous research [52] studied the influence of thermal residual stress and microscopic porosity on the transverse and longitudinal macroscopic properties of fiber-reinforced composites. This study employed a micromechanical modeling approach that incorporated artificially embedded triangular, circular, and square pentagonal pores. [53] Investigated the damage progression in carbon fiber-reinforced polymer (CFRP) generated by the effect of layup thickness on thin plates subjected to transverse tensile loading through a micromechanical modeling approach. The findings of their study indicated that, in the presence of pore defects, crack initiation takes place at the interface between the pores and the matrix, in addition to occurring at specific weak interfaces between the fibers and the matrix. The lack of resin and cohesion can have several origins, among others, a rapid gelling of the resin (resin/hardener ratio), a slow diffusion rate, etc.

Fig.7. Cross-sectional views of control specimens highlighting multiple defects in three different planes. (A) Lack of resin through fibers in the frontal plane (1), (B) good distribution of resin in the transversal plane (3), (C) good fiber-resin cohesion in the longitudinal plane (2).

Defects affect the ability to conclude the integrity of the composite. Figure7B, on the other hand, shows a cross-section along the transversal plane, showing us a surface with a well-distributed resin between the fibers,

a sign of good infusion. Figures7B-C show good fiber-resin cohesion in the longitudinal and transversal plane. Further investigation is needed to achieve better results.

3.3. Standard specimens after static tensile testing

The cross-section in the frontal plane shows a surface with a well-distributed resin between the fibers, as illustrated in the Fig.8a. Across the frontal plane, it covers the material well and has no detectable molding defects. The cross-section along the fracture plane of the specimen after tensile testing highlights the effect of static tension on the material, as shown in Fig.8b. These effects are manifested by resin cracking (F1), intralaminar delamination (F2), translaminar delamination (F3), and fiber bundle failure (F4), which is due to plastic deformation during the test. Wen *et al*. highlight that during tension, where the fiber-matrix interface starts to debond and leads to crack initiation under load [54], resulting in intralaminar delamination.

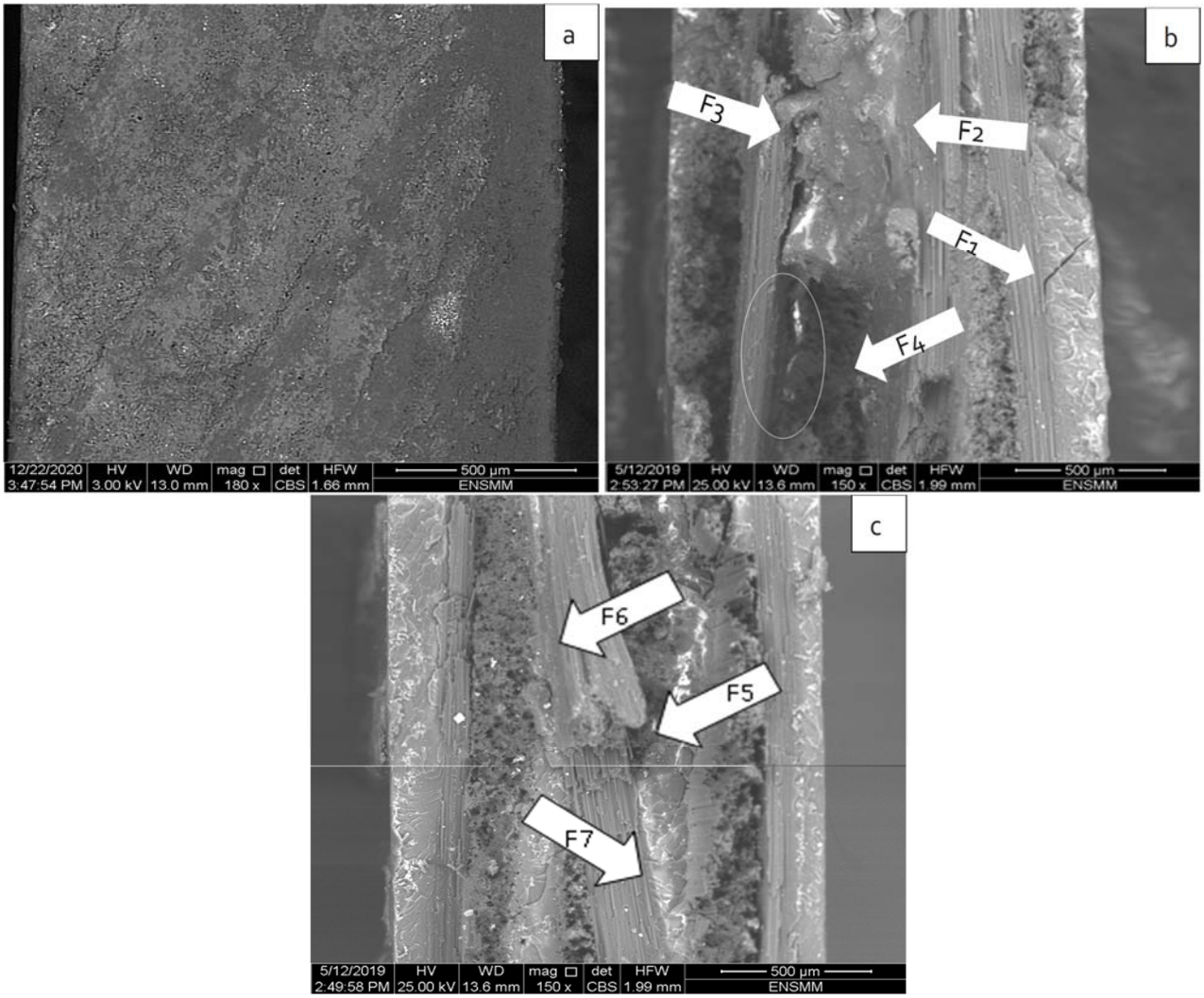

Fig.8. Cross-sectional views of the standard specimens after the static tensile test. (a) good molding infusion in the frontal plane, (b) resin cracking (F1) intralaminar, and translaminar delamination, and fiber failure (F2, F3, F4) in the fracture plane of the specimen, (c) fiber breakage, matrix decohesion, and good cohesion (F5, F6, F7) in the longitudinal plane.

The combined effect of these two types of delamination contributes to fiber breakage, which leaves a crater in the material (F4). This fiber breakage is manifested by the disappearance of fiber bundles at various levels. This demonstrates the effect of the static loading after the specimen breakage. It weakens the material and generates different types of damage. Figure 8c shows a breakage of a fiber strand along the tensile axis (F5), as well as a fiber matrix decohesion (F6). It also shows good fiber-matrix cohesion, due to effective infusion and resin-reinforcement compatibility (F7). Tensile damage is severe, damaging both the resin and the fibers.

3.4. Drilled specimens before static tensioning

Figure 9a shows the classic double interlaminar delamination at the borehole (F1 and F2). This double delamination is caused by the drill bit during drilling, which causes mode one cracking by lifting the first ply.

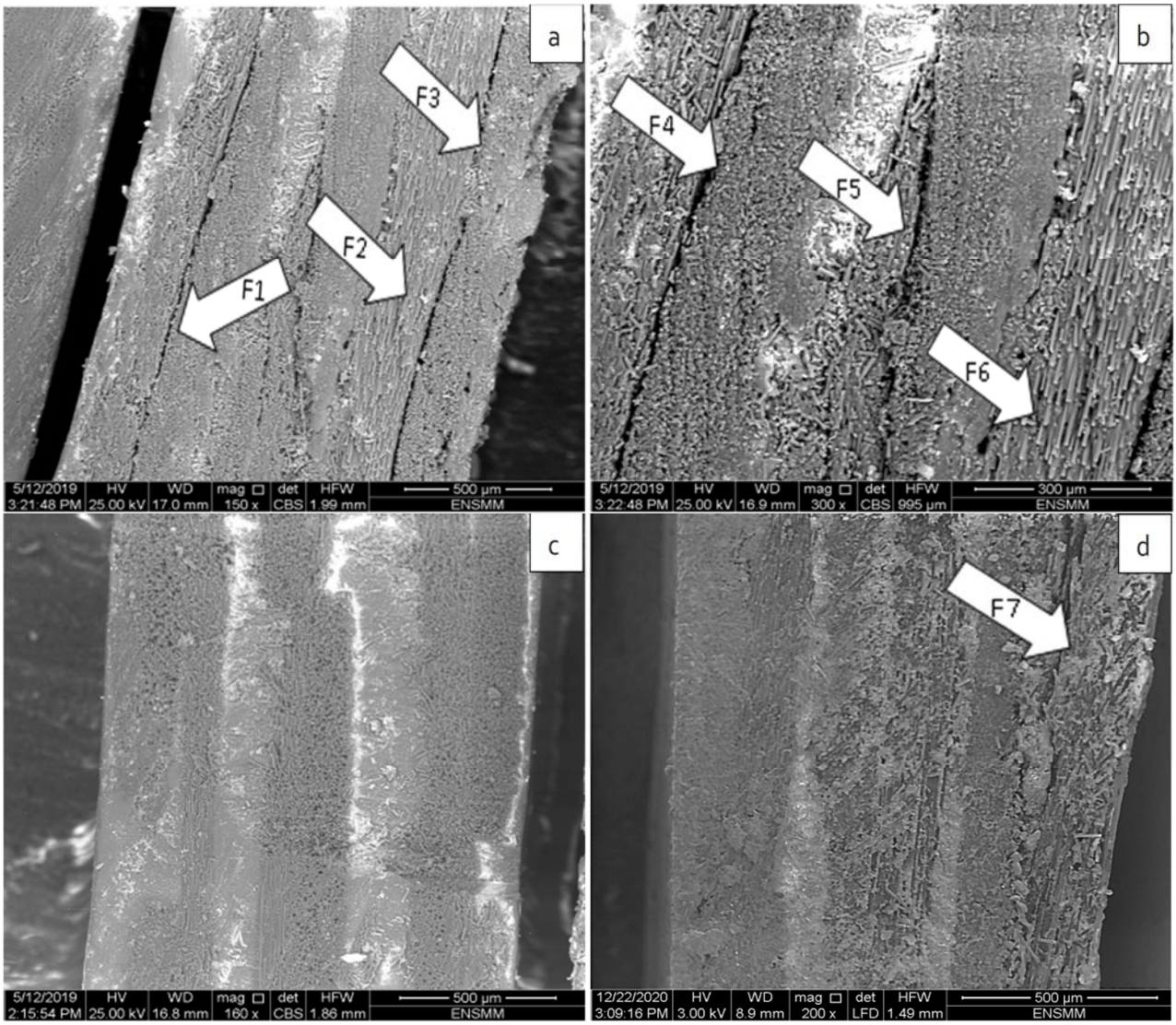

Fig.9. Cross-sectional views of the drilled specimens before the static tensile test. (a, b) double interlaminar delamination (F1, F2), and resin stripping F3 in the transversal plane of the bore hole, (c) good cohesion along the longitudinal plane, (d) the propagation of the cracking F7 in the cross-section by width.

The same phenomenon occurs when the drill exits and lifts the last ply, creating the second delamination in mode one. Aamir *et al*. confirmed that the HSS drill-bit could cause these two types of delamination, which occur between different layers and generate excessive built-up edges [55]. Ghazali *et al*. elucidate stated in their research that variations in tool material potentially mitigate both intra- and interlaminar delamination [56]. We also see resin stripping on the lower lip (F3). Figure 9b shows inter (F4) and intralaminar delaminations (F5) and brushing of the carbon fibers after they have broken in the direction of rotation and cutting of the drill bit during drilling (F6). Figure 9c shows good cohesion between the resin and the fibers along the length of the specimen. Figure 9d shows the propagation of interlaminar cracking (F7), caused by the drilling.

3.5. Drilled specimens after static tensioning

Figure 10a shows matrix cracking perpendicular to the drilling axis (F1), with the creation of an intralaminar delamination (F2), and a fiber strand pull-out (F3). Wang *et al*. reported the cause of this complex damage to the drilling, which affects the resin-matrix bonding [57]. Figure 10b shows interlaminar delamination (F4) and fiber strand push-out (F5). We also notice a fiber-matrix decohesion (F6). Figure10c shows the tearing of a fiber strand with its resin (F7) and an intralaminar delamination (F2) due to the tensile stress concentration. Additionally, the bond quality between the matrix and the strands impacts directly the occurrence of these types of delamination's which significantly decreases the mechanical performance under tension [58] Figure 10d shows interlaminar (F9, F10) and intralaminar (F11) delaminations caused by drilling with matrix failure caused by material embrittlement due to the effects of drilling and tensile stress. Drilling and tensile stresses cause extreme material degradation and embrittlement.

4. Conclusion

This study explores the various fracture surfaces of carbon fiber and c-orthocryl resin specimens. This resin is supplied by Otto Bock, a German supplier specializing in orthopedic prostheses. The resin-hardener ratio is recommended by this supplier and was respected. There are no studies on this resin when drilling and tensioning. It is therefore difficult to make comparisons with the various bibliographical studies. The results of this composite can be considered as new. And can be cited as a new reference, showing that the material undergoes various degradations across different facies, an aspect from which several conclusions can be drawn:

Intralaminar delamination occurs in both drilled and standard specimens after tensioning. In the drilled specimens, it comes along with fiber tearing and interlaminar delamination due to fiber strand push-pull-out by the drill bit on the longitudinal plane vertically with the drilling mechanism.

Translaminar delamination is identified as the damage that occurs after loading the specimens, specifically in the transverse plane perpendicular to the loading direction. This damage is due to the generation of tensile stress, which leads to resin-fiber decohesion.

Matrix cracking, recognized as advanced damage, occurs in c-orthocryl resin. This is attributed to testing in both specimens, which revealed shortages in resin-fiber cohesion in standard specimens before tensioning in the frontal and longitudinal planes in certain regions, despite sufficient cohesion across all surfaces.

The combined effect of drilling and pulling of carbon-c-orthocryl composite generates the same degradation as during pulling and drilling induced micro damages such as inter-intralaminar delamination, matrix cracks, and fiber breakage as a precursor for the tensile loading This is further supported by the absence of translaminar delamination in the drilled specimens which ruins the material by shearing the fibers at different levels.

This composite shows good performance in terms of mechanical properties, with an average ultimate tensile strength of *437.539 MPa* before it fractures. A maximum strain of *1.7%*, as well as the composite, demonstrates that has good cohesion Despite the infusion molding defects which has certain disadvantages for the final orthopedic socket, the drilling for this composite with HSS twist drill-bit has reduced the average tensile strength by *17.42%* from *437.539 MPa* to *361.286 MPa* and the strain failure has reduced by *52%* dropping from *1.7%* to *0.8%* the hole acts as the initiation point for stress propagation and a catastrophic failure,

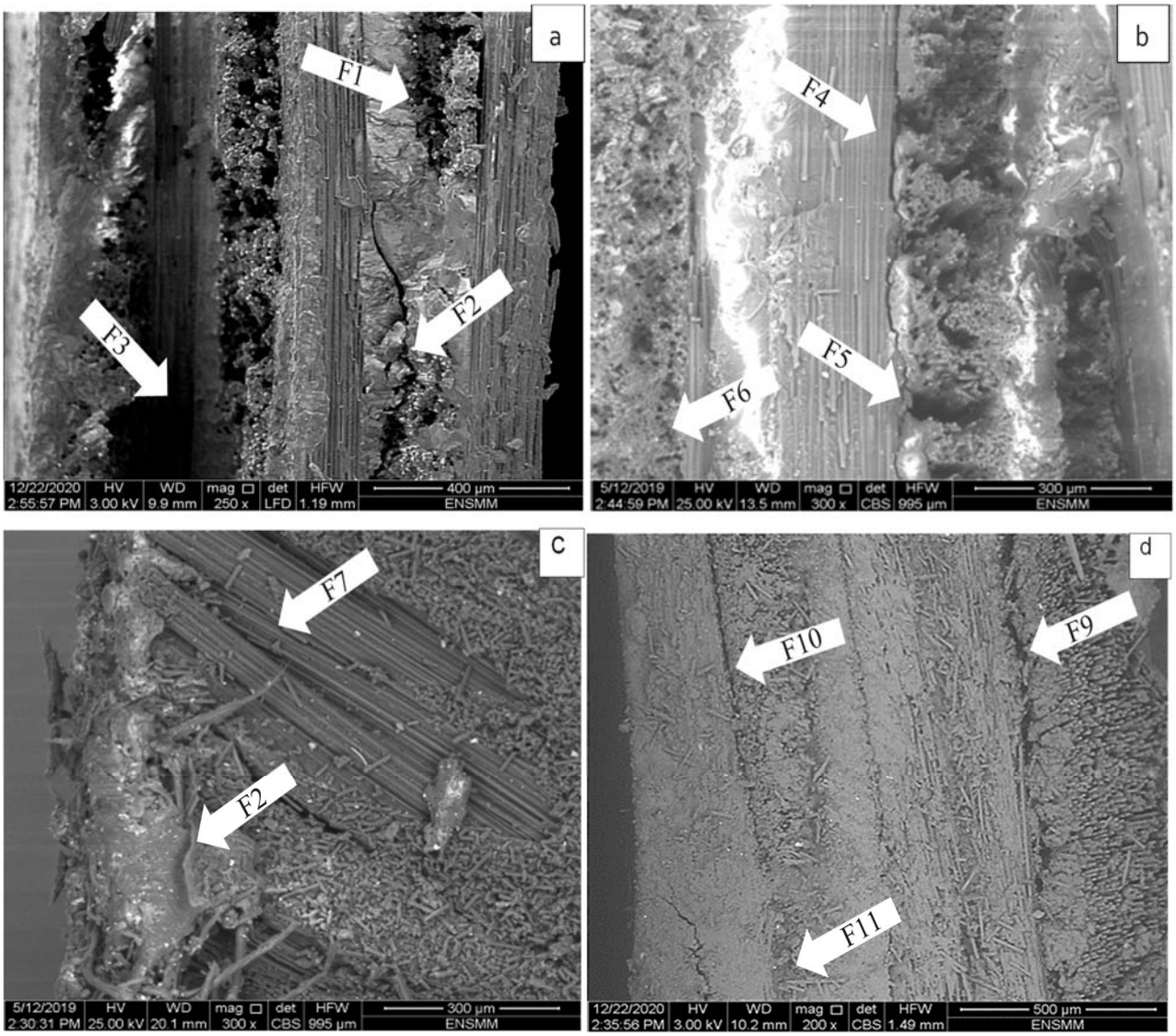

Fig.10. Cross-sectional views of the drilled specimens after the static tensile test. (a) matrix cracking F1 with intralaminar delamination and fiber strand pull-out (F2, F3) in the transverse plane by width, (b) interlaminar delamination with fiber push-out (F4, F5) in the longitudinal plane according to length, (c) fiber tearing (F7) in the cross-section (4) fracture plane of the specimen, (d) inter and intralaminar delamination (F9, F10, F11) in the transversal plane at the bore hole.

the Charpy impact test demonstrates that this material has an average impact toughness of approximately $0.075\ J / mm^2$. Indeed, a micro effect in terms of delamination, which goes along with the one cited in the bibliography, and there is poor wetting of the carbon fibers by the c-orthocryl resin, which can be corrected by adjusting the moulding techniques for obtaining the material. Additional investigation is necessary. Future research will involve conducting more detailed mechanical tests, along with an upgraded amount of retarder up to *3%*, to enhance our comprehension of the material's properties and expand its potential applications.

Acknowledgments

We would like to thank our partners for their contribution and for making their staff and resources available to us. We start with the ONAAPH (National Office of Equipment and Accessories for Disabled Patients) Annaba, for having made available to us fiber-resin for the composite manufacturing, the necessary equipment, as well as a contribution of their technicians for the realization of the laminated plates. We would also like to thank the personnel in charge for the generous assistance and the support that we received when preparing the specimens.

Nomenclature

CFRP - carbon fiber reinforced polymer
E - Young modulus
F (1-11) - defect area
HSS - high-speed steel
hrs - hours
LR3MI - Laboratoire de Recherche Mecanique et Materiaux et Maintenance Industrielle
ONAAPH - Office National d'Appareillage et Accessoires pour Personnes Handicapées
SEM - scanning electron microscope
S_0 - initial surface of the specimen
T - temperature
t - time
v - impact speed $\left(mm^2\right)$
W / S_0 - absorbed energy (J/mm^2)
W - impact energy $\left(J\right)$
ε - uniaxial strain (%)
σ - uniaxial stress $\left(MPa\right)$
σ_{max} - ultimate tensile strength $\left(MPa\right)$

References

[1] Gopalakrishnan S. (2012): *A public health perspective of road traffic accidents.*– J. Fam. Med. Prim. Care, vol.1, No.2, pp.144-150, https://doi.org/10.4103/2249-4863.104987.

[2] Peden M. and Sminkey L. (2004): *World Health Organization dedicates World Health Day to road safety.*– Inj. Prev., vol.10, No.1, pp.67-67, https://doi.org/10.1136/ip.2004.005405.

[3] Jindal A. and Mukherji S. (2005): *World report on road traffic injury prevention.*– Med. J. Armed Forces India, vol.61, No.2, pp.91-92, https://doi.org/10.1016/S0377-1237(05)80135-2.

[4] Seif M., Edalat S., Shirazi M.A., Alipouri S. and Bayati M. (2024): *Prediction of the burden of road traffic injuries in Iran by 2030: Prevalence, death, and disability-adjusted life years.*– Chin. J. Traumatol., vol.27, No.3, pp.242-248, https://doi.org/10.1016/j.cjtee.2024.02.004.

[5] Berthelot J.-M. (2012): *Matériaux Composites: Comportement Mécanique et Analyse des Structures.*– Paris: Unknown Publisher, pp.637.

[6] Pomázi Á. and Toldy A. (2019): *Multifunctional gelcoats for fiber reinforced composites.*– Coatings, vol.9, No.3, 173, https://doi.org/10.3390/coatings9030173.

[7] Kinvi-Dossou G.R. (2018): *Étude de la résistance à l'impact et de l'endommagement des composites stratifiés à matrice Elium acrylique: caractérisation expérimentale et modélisation numérique multi-échelle.*– PhD Thesis, University of Lille, France.

[8] Gouda P.S.S., Kudari S.K., Prabhuswamy S. and Jawali D. (2011): *Fracture toughness of glass-carbon (0/90), fiber reinforced polymer composite: An experimental and numerical study.*– J. Miner. Mater. Charact. Eng., vol.10, No.8, pp.671-682, https://doi.org/10.4236/jmmce.2011.108052.

[9] Goh J.C.H., Lee P.V.S. and Ng P. (2002): *Structural integrity of polypropylene prosthetic sockets manufactured using the polymer deposition technique.*– Proc. Inst. Mech. Eng. Part H, J. Eng. Med., vol.216, No.4, pp.359-368, https://doi.org/10.1243/095441102321032157.

[10] Gariboldi F., Scapinello M., Petrone N., Migliore G.L., Teti G. and Cutti A.G. (2023): *Static strength of lower-limb prosthetic sockets: An exploratory study on the influence of stratigraphy, distal adapter and lamination resin.*– Med. Eng. Phys., vol.114, p.103970, https://doi.org/10.1016/j.medengphy.2023.103970.

[11] Campbell A.I., Sexton S., Schaschke C.J., Kinsman H., McLaughlin B. and Boyle M. (2012): *Prosthetic limb sockets from plant-based composite materials.*– Prosthet. Orthot. Int., vol.36, No.2, pp.181-189, https://doi.org/10.1177/0309364611434568.

[12] Greenhalgh E.S. (2009): *Failure Analysis and Fractography of Polymer Composites.*– Cambridge: Woodhead Publishing, pp.595, https://doi.org/10.1533/9781845696818.

[13] Madhukar M.S. and Drzal L.T. (1992): *Fiber-matrix adhesion and its effect on composite mechanical properties. III. Longitudinal (0°) compressive properties of graphite/epoxy composites.*– J. Compos. Mater., vol.26, No.3, pp.310-333, https://doi.org/10.1177/002199839202600301.

[14] Lee B.L. and Holl M.W. (1996): *Effects of moisture and thermal cycling on in-plane shear properties of graphite fibre-reinforced cyanate ester resin composites.*– Compos. Part A Appl. Sci. Manuf., vol.27, No.11, pp.1015-1022, https://doi.org/10.1016/1359-835X(96)00027-9.

[15] Boufaida Z. (2015): *Analyse des propriétés mécaniques de composites taffetas verre/matrice acrylique en relation avec les propriétés d'adhésion des fibres sur la matrice.*– PhD Thesis, University of Oran, Algeria, pp.213.

[16] Pvr G.K. and Devi K.D. (2025): *Influence of manufacturing parameters on the properties of 3D printed polylactic acid carbon fiber components.*– Arch. Metall. Mater., vol.70, No.1, pp.97-104, https://doi.org/10.24425/amm.2025.152523.

[17] Bergeret A. and Krawczak P. (2006): *Liaison renfort/matrice– Définition et caractérisation.*– Plast. Compos., vol.1, p.5305, https://doi.org/10.51257/a-v1-am5305.

[18] Dong C. and Davies I.J. (2012): *Optimal design for the flexural behaviour of glass and carbon fibre reinforced polymer hybrid composites.*– Mater. Des., vol.37, pp.450-457, https://doi.org/10.1016/j.matdes.2012.01.021.

[19] Han S.H., Oh H.J. and Kim S.S. (2014): *Evaluation of the impregnation characteristics of carbon fiber-reinforced composites using dissolved polypropylene.*– Compos. Sci. Technol., vol.91, pp.55-62, https://doi.org/10.1016/j.compscitech.2013.11.021.

[20] Geier N., Pereszlai C., Poór D.I. and Balázs B.Z. (2021): *Drilling of curved carbon fibre reinforced polymer (CFRP) composite plates.*– Procedia CIRP, vol.99, pp.404-408, https://doi.org/10.1016/j.procir.2021.03.057.

[21] Turla P., Kumar S.S., Reddy P.H. and Shekar K.C. (2014): *Processing and flexural strength of carbon fiber and glass fiber reinforced epoxy-matrix hybrid composite.*– Int. J. Eng. Res. Technol., vol.3, No.4, pp.394-398, https://doi.org/10.17577/IJERTV3IS040781.

[22] Ihiawakrim D. (2019): *Étude par les techniques avancées de microscopie électronique en transmission de matériaux fragiles.*– PhD Thesis, pp.173.

[23] Ledru Y., Piquet R., Michel L. and Schmidt F. (2009): *Quantification 2-D et 3-D de la porosité par analyse d'images dans les matériaux composites stratifiés aéronautiques.*– JNC 16, vol.16, pp.10-12.

[24] Gliesche K., Hübner T. and Orawetz H. (2005): *Investigations of in-plane shear properties of ±45°-carbon/epoxy composites using tensile testing and optical deformation analysis.*– Compos. Sci. Technol., vol.65, No.1, pp.163-171, https://doi.org/10.1016/j.compscitech.2004.05.004.

[25] Goutham K.B., Mathew N.T. and Vijayaraghavan L. (2021): *Delamination and tool wear in drilling of carbon fabric reinforced epoxy composite laminate.*– Mater. Today Proc., vol.50, pp.823-829, https://doi.org/10.1016/j.matpr.2021.06.030.

[26] Romhány G. and Szebényi G. (2012): *Interlaminar fatigue crack growth behavior of MWCNT/carbon fiber reinforced hybrid composites monitored via newly developed acoustic emission method.*– Express Polym. Lett., vol.6, No.7, pp.572-580, https://doi.org/10.3144/expresspolymlett.2012.60.

[27] Szebényi G., Magyar B. and Iványicki T. (2017): *Comparison of static and fatigue interlaminar testing methods for continuous fiber reinforced polymer composites.*– Polym. Test., vol.63, pp.307-313, https://doi.org/10.1016/j.polymertesting.2017.08.033.

[28] Gupta S., Pal S. and Ray B.C. (2022): *An analysis on tensile and flexural loading response for unidirectional CFRP laminate with cutout/hole: Geometrical design effect on the material strength.*– J. Appl. Polym. Sci., vol.139, No.12, p.53139, https://doi.org/10.1002/app.53139.

[29] Li Y., Wang B. and Zhou L. (2023): *Study on the effect of delamination defects on the mechanical properties of CFRP composites.*– Eng. Fail. Anal., vol.153, p.107576, https://doi.org/10.1016/j.engfailanal.2023.107576.

[30] Chen R., Li S., Zhou Y., Qiu X., Li P., Zhang H. and Wang Z. (2023): *Damage formation and evolution mechanisms in drilling CFRP with prefabricated delamination defects: Simulation and experimentation.*– J. Mater. Res. Technol., vol.26, pp.6994-7011, https://doi.org/10.1016/j.jmrt.2023.09.065.

[31] Tao C., Qiu J., Yao W. and Ji H. (2016): *The effect of drilling-induced delamination on tensile strength and prediction of residual strength of carbon fiber-reinforced polymer laminate.*– J. Compos. Mater., vol.50, No.24, pp.3373-3384, https://doi.org/10.1177/0021998315620292.

[32] Zhang J., Chaisombat K., He S. and Wang C.H. (2012): *Hybrid composite laminates reinforced with glass/carbon woven fabrics for lightweight load-bearing structures.*– Mater. Des., vol.36, No.1, pp.75-80, https://doi.org/10.1016/j.matdes.2011.11.006.

[33] Bhudolia S.K., Gohel G., Leong K.F. and Barsotti R. (2020): *Investigation on ultrasonic welding attributes of novel carbon/Elium® composites.*– Materials, vol.13, No.5, p.1117, https://doi.org/10.3390/ma13051117.

[34] Yang S., Lü Y., Zhang C., Yang L. and Xu M. (2023): *Enhancement of interfacial properties of carbon fiber reinforced polyphenylene sulfide resin by sulfur treatment.*– J. Appl. Polym. Sci., vol.140, No.20, https://doi.org/10.1002/app.53850.

[35] Klaisiri A., Maneenacarith A., Krajangta N., Sukkee A., Hardy N.S., Wutikhun T. and Supachartwong C. (2023): *Surface modification methods of self-cured acrylic resin repaired with resin composite using a universal adhesive.*– J. Compos. Sci., vol.7, No.9, p.360, https://doi.org/10.3390/jcs7090360.

[36] Barbera L., Korhonen H., Masania K. and Studart A.R. (2024): *Phase-separating resins for light-based three-dimensional printing of oxide glasses.*– Sci. Rep., vol.14, No.1, https://doi.org/10.1038/s41598-024-63069-w.

[37] Ottobock: *C-Orthocryl 617H55 laminating resin – Product page.*– Accessed August (2025). https://shop.ottobock.ca.

[38] Ottobock: *617P37 / 617PG37 hardener – Technical data sheet.*– Accessed August (2025). https://shop.ottobock.ca.

[39] Ottobock: *Fabrication instructions: Lamination with C-Orthocryl resins (DynamicArm technical guide).*– Accessed August (2025). https://shop.ottobock.ca/store/medias/646T5-9.1-GB-06-1602w.pdf.

[40] ISO 527-1 (1997): *Plastics - Determination of tensile properties– Part 1: General principles.*– ISO Standard, 2012 Edition.

[41] ISO 179-1 (2010): *Plastics.- Determination of Charpy impact properties.*– ISO Standard, pp.11.

[42] Huang B., Yang Y., Liu X.G. and Yue Q.R. (2023): *Study on probability model and length effect of tensile strength of unidirectional CFRP plate.*– Compos. Struct., vol.324, p.117531, https://doi.org/10.1016/j.compstruct.2023.117531.

[43] Zhang F., Ji S., Zhang H., Wang H., Wang H. and Bi Y. (2024): *Tensile performance prediction of CFRPs with voids using multiscale analysis and neural networks.*– Mater. Today Commun., vol.41, p.110462, https://doi.org/10.1016/j.mtcomm.2024.110462.

[44] Caminero M.A., Rodríguez G.P. and Muñoz V. (2016): *Effect of stacking sequence on Charpy impact and flexural damage behavior of composite laminates.*– Compos. Struct., vol.136, No.1, pp.345-357, https://doi.org/10.1016/j.compstruct.2015.10.019.

[45] Caminero M.A., García-Moreno I., Rodríguez G.P. and Chacón J.M. (2019): *Internal damage evaluation of composite structures using phased array ultrasonic technique: Impact damage assessment in CFRP and 3D printed reinforced composites.*– Compos., Part B Eng., vol.165, pp.131-142, https://doi.org/10.1016/j.compositesb.2018.11.091.

[46] Li S., Hu J. and Ren H. (2017): *The combined effects of environmental conditioning and sustained load on mechanical properties of wet lay-up fiber reinforced polymer.*– Polymers, vol.9, No.7, p.244, https://doi.org/10.3390/polym9070244.

[47] Ueda M., Cuong V.M., Yamanaka A. and Sakata K. (2020): *Tensile, compressive, and fatigue strength of a quasi-isotropic carbon fiber reinforced plastic laminate with a punched hole.*– Heliyon, vol.6, No.12, e05690, https://doi.org/10.1016/j.heliyon.2020.e05690.

[48] Yenigün B. and Kılıçkap E. (2018): *Prediction of the tensile load of drilled CFRP by artificial neural network.*– Appl. Sci., vol.8, No.4, p.549, https://doi.org/10.3390/app8040549.

[49] Mahfoud E. and Harb M. (2023): *Numerical lamb wave modeling and analysis for cure cycle shortening of carbon fiber composites.*– J. Compos. Mater., vol.57, No.9, pp.1683-1703, https://doi.org/10.1177/00219983231160874.

[50] Zhang H., Zhao G., Li X., Hao Z. and Zhong Z. (2024): *Effect of carbon nanotubes on thermoset curing and mechanical properties of carbon fiber reinforced epoxy resin laminates fabricated by self-resistance electric heating.*– Polym. Compos., vol.45, No.7, pp.6111-6124, https://doi.org/10.1002/pc.28182.

[51] Ye Y., Liu B. and Li P. (2022): *Significantly improving mechanical properties of epoxy resin-based carbon fiber-reinforced plastic composites via introducing oxazolidinone segments.*– Polym. Polym. Compos., vol.30, https://doi.org/10.1177/09673911211065196.

[52] He J., Cui X., Lua J. and Liu L. (2023): *Interplay of manufacturing-induced thermal residual stresses and microvoids in damage and failure of fiber-reinforced composites.*– Int. J. Mech. Sci., vol.242, p.108000, https://doi.org/10.1016/j.ijmecsci.2022.108000.

[53] Naderi M. and Iyyer N. (2020): *Micromechanical analysis of damage mechanisms under tension of 0°-90° thin-ply composite laminates.*– Compos. Struct., vol.234, p.111659, https://doi.org/10.1016/j.compstruct.2019.111659.

[54] Wen J., Wu Y., Hou X., Yan M. and Xiao Y. (2022): *Effect of high temperature on mechanical properties and porosity of carbon fiber/epoxy composites.*– J. Reinf. Plast. Compos., vol.42, No.19-20, pp.990-1005, https://doi.org/10.1177/07316844221143747.

[55] Aamir M., Sharif A., Zahir M.Z., Giasin K. and Tolouei-Rad M. (2023): *Experimental assessment of hole quality and tool condition in the machining of an aerospace alloy.*– Machines, vol.11, No.7, p.726, https://doi.org/10.3390/machines11070726.

[56] Ghazali M.F., Abdullah M.M.A.B., Rahim S.Z.A., Gondro J., Pietrusiewicz P., Garus S. and Osman M.S. (2021): *Tool wear and surface evaluation in drilling fly ash geopolymer using HSS, HSS-Co, and HSS-TiN cutting tools.*– Materials, vol.14, No.7, p.1628, https://doi.org/10.3390/ma14071628.

[57] Wang C., Guan S., Sabbrojjaman M. and Tafsirojjaman T. (2023): *Bond performance of CFRP strands to grouting admixture for prestressed structure and development of their bond-slip constitutive models.*– Polymers, vol.15, No.13, p.2906, https://doi.org/10.3390/polym15132906.

[58] Kim K.M., Park S., Song B. and Yoon S. (2024): *Evaluation of the flexural behavior of one-way slabs by the amount of carbon grid manufactured by adhesive bonding.*– Polymers, vol.16, No.19, p.2690, https://doi.org/10.3390/polym16192690.

Received: July 20, 2025
Revised: December 2, 2025